

Online reliability assessment of energy systems based on a high-order extended-state-observer with application to nuclear reactors

Zhe Dong ^{a,b,*}, Bowen Li ^a, Junyi Li ^a, Xiaojin Huang ^a, Zuoyi Zhang ^a

^a Institute of Nuclear and New Energy Technology (INET), Collaborative Innovation Center of Advanced Nuclear Energy Technology of China, Key Laboratory of Advanced Reactor Engineering and Safety of Ministry of Education, Tsinghua University, Beijing, 100084, China

^b State Key Laboratory of Nuclear Power Safety Monitoring Technology and Equipment, Shenzhen, Guangdong, 518172, China



ARTICLE INFO

Keywords:

Energy system reliability
Online reliability estimation
Extended-state-observer

ABSTRACT

Online reliability assessment is not only crucial for the safe and stable operation of energy systems but also meaningful for guaranteeing satisfactory economic competitiveness. Due to the system reliability can be determined by the failure-rate and operation time, the central in online reliability assessment of energy systems is the evaluation of failure-rate. Further, it can be seen that the deviations of actual responses of process variables from their expectations reflect the effect of total disturbance, and large deviations usually denote the existence of the degradation of system reliability. Hence, the failure-rate can be evaluated based on the estimation of total disturbance and its differentiation. In this paper, a high-order extended state observer (HO-ESO) is proposed for the nonlinear dissipative system representing typical energy system dynamics, which provides globally bounded observations for not only system state-variables but also the total disturbance and its differentiation. Then, the evaluations of both the failure-rate and the system reliability can be given online based on the estimation provided by the HO-ESO. Further, this HO-ESO-based online reliability assessment method is applied to the health monitoring of pressurized water reactor (PWR). After checking the dissipation condition of PWR, the HO-ESO of PWR is designed, and the simulation results show the feasibility and effectiveness.

1. Introduction

Reliability is the fundamental component of the energy industry, which deeply influences the safety, security and economy of energy systems such as nuclear plants, wind turbines, fuel cells and many research results have been given for the reliability analysis of energy production and transmission systems. In Ref. [1], based on two large non-public emergency diesel generator (EDG) operational data, it is shown that the single EDG configurations are only 80% likely to provide power for the duration of a two-week grid outage, which means that maintenance of EDG is crucial to keep a high level of reliability. In Ref. [2], the study on renewable integration impact assessment shows that the renewable capacity is not primarily given by the amount of resource, but is given by reliability degradation of bulk electric system caused by the intermittence of renewable generation. In Ref. [3], it is pointed out that the lifespan is an important disadvantage of fuel cells, and it is recommended to incorporate health monitoring and prognostics to the development of fuel cell technology so as to give suitable

competitive advantage when compared with other on-clean energy solutions. In Ref. [4], it is shown that high availability of smart grids is not only given by the capability of load-balancing but also given by the level of system reliability, and availability can be guaranteed by solving reliability optimization Problem with the load balancing as a constraint. In Ref. [5], it is recommended that more research effort should be given for the reliability-centered maintenance of distribution systems so as to increase the energy availability, quality, and safety while decreasing the operation and maintenance (O&M) cost. The analysis in Ref. [6] shows that condition-based maintenance (CBM) of wind turbines is the basis of reducing the O&M cost, and the electrical and control components are the emphasis of health monitoring since their malfunction causes more than 75% of the total downtime. Similarly, in Ref. [7], it is also suggested that CBM is important for mechanical equipment, where the prognostics is a crucial basis of CBM aiming at providing the estimation of residual useful life (RUL). For the reliability of fuel cells, the research in Ref. [8] further shows that degradation of lifespan is mainly caused by the frequent varying of load connected to the fuel cells, and health

* Corresponding author. Institute of Nuclear and New Energy Technology (INET), Collaborative Innovation Center of Advanced Nuclear Energy Technology of China, Key Laboratory of Advanced Reactor Engineering and Safety of Ministry of Education, Tsinghua University, Beijing, 100084, China.

E-mail address: dongzhe@mail.tsinghua.edu.cn (Z. Dong).

monitoring is meaningful to reduce the fault rate. For photovoltaic (PV) systems, it is also emphasized in Ref. [9] that health monitoring is important in guaranteeing reliability, where the health monitoring can be realized by comparing the measurements and the estimations of some key process variables. It is further point out in Ref. [10] that the inverters are most costly in the maintenance of PV systems, responsible for between 43% and 70% of the service ticket, and the monitoring of inverters is the emphasis of PV system monitoring. In Ref. [11], the reliability risk mitigation of the free air cooling system of data centers are discussed, and the result shows that the prognostics-based approach can provide early warnings of failures and thus reduce the unscheduled downtime of data centers.

From the above work about energy system reliability, it can be seen that online reliability assessment (ORA) is the basis for condition-based maintenance which is helpful for improving system reliability. Practically, to assess the energy system reliability online, it is necessary to involve the use of physical or risk indicators that can effectively denote reliability degradation [12]. Usually, the deviations of direct or indirect process variables can be adopted for denoting the degradation. In Ref. [13], it is stated that the degradation of fuel cells must induce the deviation of process variables that can be measured directly or indirectly, which means that the deviation of process variables can be utilized as the indicator of reliability degradation. In Ref. [14], the potential of frictional energy, which can be measured indirectly, is adopted for the reliability assessment of wind turbine gearboxes. In addition, some virtual parameters can also be used for indicating system reliability, and a virtual parameter is usually given by a set of process variables reflecting an operating feature. In Ref. [15], the equivalent total moment of inertia of a local electric grid is adopted for indicating the grid stability in the context of high renewable integration, where the grid stability is tightly related with the operation reliability. After obtaining a proper indicator of system reliability degradation, the reliability assessment (RA) methods should be developed, which is a hot spot in energy system health monitoring. During the past decade, several advanced RA methods have been proposed, which can be classified to physics-based methods, data-based methods and state-observation-based methods.

Physics-based reliability assessment methods give the system reliability estimations based on the process models. The failure mechanism model, which can be given by either theoretical equations or experimental data. In Ref. [16], a multi-state physics model was proposed for the degradation modeling of nuclear power plant (NPP) piping systems, which describes the degradation process by transitions among discrete states, such as no damage, micro-crack, flaw and rupture, with physics modeling by equations to describe the continuous degradation process within the states. In Ref. [17], probabilistic fracture mechanics was applied to assess the reliability of cracked components in NPP piping. In Ref. [18], the physical model gives an algebraic relationship between residual useful life (RUL) and the number of charging cycles of lithium-ion batteries are proposed, which is then applied in conjunction with the classical recursive least-square (RLS) method to estimate the RUL. In Ref. [19], the failure-rate model of wind-energy system is given based on the assumption of using the reliability degradation characteristics given by the bathtub curve, and the parameters of this model can be estimated online from the operation data. In Ref. [20], the data from accelerated life testing experiment is adopted to train an artificial neural network (ANN) model so as to predict both the RUL and reliability of the instrument and control (I&C) cables of a nuclear power plant (NPPs). Moreover, the process models describing the balances of mass, energy and momentum are also usually adopted for system reliability assessment. In Ref. [21], the steady mass, energy and momentum balance equations of thermal processes are directly applied for the measurement data reconciliation so as to indicate and detect the reliability degradation of instrumentation system. In Ref. [22], based on defining the supply reliability of a natural gas pipeline network as the probability of successfully providing the required demand of gas, a dynamical model is

proposed through integrating stochastic processes, graph theory and pipeline thermal-hydraulics so as to assess the supply reliability. In Ref. [23], it is first suggested that the dynamical model of an energy system should be composed of the deterministic part given by the physical balances and the stochastic part reflecting the characteristics of degradation, and then a stochastic hybrid fault tree automaton is proposed to assess the reliability of renewable energy system through numerical simulation. Actually, stochastic hybrid automaton is an effective simulation based method to assessing the reliability of complex energy system such as the steam generators [24], and Monte Carlo method is usually adopted for the corresponding reliability calculation [25,26]. From the above introduction about physics-based reliability assessment methods, it can be seen that the models for failure mechanism or for system dynamics are necessary. However, not all the engineering systems have clearly known failure mechanics or accurate dynamical models, especially for those complex energy systems having multiple correlated failure-modes. Hence, physics-based methods are more suitable for the systems of which the failure mechanisms are specifically clear or the dynamical models are accurate enough.

Data-driven methods provide reliability estimation based on the fact that the exacted features of condition monitoring data vary with the degradation level. Data driven methodologies are useful when a large quantity of noisy data needs to be transformed into a piece of logical information to estimate the reliability online. In Ref. [27], a regression model with parameters given by the principle component analysis (PCA) method is proposed to evaluate the reliability of passive decay heat removal systems of NPPs. In Ref. [28], an ANN based response surface (ANNBRS) method is developed for reliability assessment of the passive safety systems in a nuclear plant, where the PCA is used to extract the training data of the ANN model from the operation data of NPP. In Ref. [29], a data driven reliability assessment method is proposed for the sensors in a vapor compression system, where the subtractive clustering is used for classifying and recognizing the operation conditions, the PCA is adopted for fault detection, and the statistical quantities T^2 and SPE are combined together to evaluate the measurement reliability. In Ref. [30], it is reported that both the supervised and unsupervised statistical learning methods can be applied for the data-driven online reliability evaluation of the structure of offshore wind turbines. In Ref. [31], an online dynamic fuzzy neural network (OD-FNN) based machine health monitoring method is given, where the parameters of the OD-FNNs are trained based on the classical recursive least-square (RLS) estimator. In Ref. [32], two step data-driven RUL estimation method in aeronautics is proposed, where the first step is to give the RUL estimation based on an unsupervised method called nearest neighbors, and the second step is to use the Kalman filter to improve the estimation precision. In Ref. [33], the support vector regression (SVR) is applied for predicting the unmeasurable state of health (SOH), e.g. the capacity of a battery or the bearing vibration of a gear-box, which determines the RUL to a large extent. In Ref. [34], the SVR is integrated with another supervised learning method called variable neighborhood search (VNS) so as to give the reliability estimation, which shows a superior performance than other techniques such as the multi-layer perception and radial basis function (RBF) network. In Ref. [35], the deep convolution neural network (DCNN) is applied to predict the RUL without any prior expertise knowledge, and the input to the DCNN is the normalization of the raw collected data. Recently, the research on data-driven reliability assessment have entered to the implementation stage. In Ref. [36], the ANN, SVR and some other data-driven artificial intelligence (AI) techniques have been applied to build a smart support system for diagnosing severe accidents for NPPs. Now, it can be seen that data-driven reliability methods are widely utilized in the reliability assessment of complex energy system such as nuclear reactors, wind turbines, lithium-ion batteries and fuel cells, where the relationship between the reliability indicator and process variables is mined from the abundant operation data. Usually, the unsupervised learning methods such as the PCA are utilized for extracting the training samples from the operation

data, and supervised learning methods such as the ANN and SVR are applied for RUL prediction.

From the above introduction about the development status of physics-based and data-based methods, it can be seen that physics-based methods depend heavily on the accurate models of either the failure mechanism or the process dynamics, while the data-driven methods need to handle big operation data without any prior knowledge about system dynamics and to give the relationship between process variables and reliability indicator. However, it may be more effective to assess the system reliability by combining the plant model and the operation data, which is motivated by the fact that a skilled plant operator usually assesses the plant operation state based on not only the measurements but also prior knowledge about system dynamics. This idea stimulates the research on the state-observer-based reliability assessment method, where operational data are utilized to update some special terms of the model so as to estimate those unmeasurable variables or reliability indicators. In Ref. [37], the state-of-charge (SoC) of lithium-ion batteries, which directly reflects the battery reliability, is regarded as an unmeasurable state-variable, and then is estimated by the use of the unscented Kalman filter (UKF) with a steady error of 1.83%. In Ref. [38], a proportional integral state-observer is designed to estimate the cooling load of the telecommunication cooling system, where the variation of unmeasurable cooling load can reflect the operation reliability to some extent. In Ref. [39], the poisons reactivity in the pressurized water reactor (PWR) is estimated by a high order sliding mode observer, which can be utilized to observe the concentrations of poisons in the PWR. In Ref. [40], an adaptive state-observer is proposed for the globally bounded estimations of both the averaged fuel temperature and total reactivity, which is meaningful for the operation monitoring of nuclear reactors. By combining both the nominal model and the operation data, the observer-based approaches are able to give the estimation of some key unmeasurable variables that can be used to indicate the system reliability. However, the observer-based method can only give the estimations to the state-variables and/or parameters based on the nominal model. Actually, there exists a mismatch between the nominal model for designing state-observer and the practical system dynamics, which can heavily deteriorate the state-observation performance and may result in an unacceptable reliability evaluation.

The modeling mismatch, which can be also called total disturbance, is able to reflect the deviation of current operation state from the state in nominal conditions. Hence, it can be seen that if the disturbance can be observed online, then the corresponding observation can be directly used for process reliability assessment, which is the basic idea of disturbance-observer-based reliability assessment method. Although the disturbance-observation-based method may have some attracting virtues, there is still very limited works in this field, and the current results focus on providing the basic techniques for disturbance observation. In Ref. [41], a nonlinear disturbance observer (DO) is proposed for mechanical systems described by state-space models, and then the disturbance-observer-based-control (DOBC) method is developed in Ref. [42] which can guarantee globally asymptotically bounded closed-loop stability at least. Very recently, the DO design method has been extended to those nonlinear system represented by input-output models [43]. The extended state-observer (ESO) is another effective method for estimating the process disturbance [44,45], whose basic idea is to regard the total disturbance as an extended state-variable while guaranteeing satisfactory convergence by high observer gains. Based on the ESO, the active disturbance rejection control (ADRC) is proposed, which cancelling the disturbance by feedback control based on the disturbance estimation provided by ESO [44]. The ESO has already been widely applied to the motion control of many industrial mechanical equipment, e.g. the Stewart platform [46] and the magnetic rodless pneumatic cylinder [47]. Usually, the ESO is suitable for those systems whose dynamics can be given by the strict feedback form. In Ref. [48], an ESO with the structure of nuclear reactor dynamics is proposed to estimate the total disturbance, which can provide satisfactory

performance in both the critical and subcritical condition. Although both ESO and DO can provide strong performance in disturbance estimation, however, for the online reliability assessment and condition monitoring, it is meaningful to give the estimation to not only the disturbance itself but also its rate of change, since the changing rate of disturbance directly reflects the rate of losing the balances of force, heat, power and etc.

In this paper, a disturbance-observer-based online reliability assessment method is newly proposed for energy systems. Since the dynamics of most energy systems can be represented by nonlinear dissipative systems, a high-order ESO (HO-ESO) of nonlinear dissipative systems is first proposed, which can provide the globally asymptotically bounded estimation to the total disturbance and its rate of change. Then, by defining the failure-rate based on the changing rate of total disturbance, the operation reliability of general energy systems can then be evaluated online directly based on the estimations provided by the HO-ESO. Furthermore, this HO-ESO-based reliability estimation method is applied to the health monitoring of pressurized water reactors (PWRs). After checking the dissipation condition of PWR dynamics, the high order ESO to estimate the total disturbances and their differentiation in the channels of neutron kinetics and thermal-hydraulics are given. Numerical simulation related to a special PWR, i.e., the nuclear heating reactor (NHR), is performed, and the simulation results in the cases of normal power decrease, step decrease of reactivity and load rejection are given, which show the feasibility and satisfactory performance of this ESO-based reliability estimator.

2. Problem formulation

Consider the energy systems with dynamics taking the form as

$$\begin{cases} \dot{\mathbf{y}} = \mathbf{f}_o(\mathbf{y}, \mathbf{z}) + \mathbf{G}(\mathbf{y})\mathbf{u} + \xi \\ \dot{\mathbf{z}} = \mathbf{f}_i(\mathbf{y}, \mathbf{z}) \end{cases} \quad (1)$$

where

$$\mathbf{x} = [\mathbf{y}^T \quad \mathbf{z}^T]^T \in \mathbb{R}^n, \quad (2)$$

is the state-vector with $\mathbf{y} \in \mathbb{R}^m$ measurable and $\mathbf{z} \in \mathbb{R}^{n-m}$ unmeasurable, $\mathbf{u} \in \mathbb{R}^l$ is the control input, $\mathbf{f}_o \in \mathbb{R}^m$, $\mathbf{f}_i \in \mathbb{R}^{n-m}$ and $\mathbf{G} \in \mathbb{R}^{m \times l}$ are given norm-bounded functions, $\xi \in \mathbb{R}^m$ is the total disturbance.

The total disturbance ξ denotes the mismatch between disturbed model (1) with its nominal model given by

$$\begin{cases} \dot{\mathbf{y}} = \mathbf{f}_o(\mathbf{y}, \mathbf{z}) + \mathbf{G}(\mathbf{y})\mathbf{u}, \\ \dot{\mathbf{z}} = \mathbf{f}_i(\mathbf{y}, \mathbf{z}). \end{cases} \quad (3)$$

For industrial energy systems, nominal model (3) describes the balances of mass, momentum and energy under expected conditions. Under abnormal conditions, due to the influence of exterior and interior disturbances, system dynamics should deviate from the nominal model, and total disturbance ξ is used to describe the deviation from expected balances. Practically, since the disturbed model deviates from its nominal dynamics with a bounded rate, it is not loss of generality to assume that total disturbance ξ satisfies

$$\begin{cases} \dot{\xi} = \zeta, \\ \zeta = \mathbf{d}, \end{cases} \quad (4)$$

where

$$\|\mathbf{d}\|_2 \leq D, \quad (5)$$

ζ is the changing rate of total disturbance ξ , $\mathbf{d} \in \mathbb{R}^m$ is the changing acceleration of ξ , and D is a given bounded positive constant. It can be seen from models (1), (3) and (4) that ζ describes the rate of losing the nominal balances of mass, momentum and energy. Further, it can be seen from (4) and (5) that disturbance changing acceleration \mathbf{d} is assumed to be bounded, which can be generally satisfied for the

practical energy systems, otherwise, total disturbance can step to infinity.

Moreover, since all the energy producing and consuming systems in the real world are dissipative, it is reasonable to suppose that disturbed energy system dynamics (1) is strictly dissipative, i.e. there exists a positive-definite function $S(\mathbf{x})$ called storage function so that

$$\left[\frac{\partial S(\mathbf{x})}{\partial \mathbf{x}} \right]^T \mathbf{f}(\mathbf{x}) = -Q(\mathbf{x}) < 0, \quad (6)$$

where

$$\mathbf{f}(\mathbf{x}) = \begin{bmatrix} \mathbf{f}_o(\mathbf{y}) \\ \mathbf{f}_i(\mathbf{z}) \end{bmatrix}, \quad (7)$$

and Q is positive-definite function called dissipation rate.

It is well known that, in the engineering, total disturbance ξ is mainly induced by the deterioration of process equipment as well as sensors and actuators, which is tightly related to operation reliability R determined by

$$\frac{dR}{dt} = -r_f R(t), \quad R(0) = R_0, \quad (8)$$

where r_f is the failure-rate measuring the deterioration rate of operation reliability R . Usually, since the initial reliability R_0 satisfies $R_0 = 1$, the solution of differential equation (8) is

$$R(t) = R_0 \exp(-r_f t) = \exp(-r_f t). \quad (9)$$

Suppose that the failure-rate r_f is given by the disturbance changing rate ζ through

$$r_f = \sum_{k=1}^m |\mathbf{d}\zeta(\zeta_k, b_k, l_k)|, \quad (10)$$

where

$$\mathbf{d}\zeta(\zeta_k, b_k, l_k) = \begin{cases} l_k(\zeta_k - b_k), & \zeta_k \geq b_k, \\ 0, & -b_k < \zeta_k < b_k, \\ l_k(\zeta_k + b_k), & \zeta_k \leq -b_k, \end{cases} \quad (11)$$

is a deadzone function, and both b_k and l_k are given positive constants. From (10) and (11), failure-rate r_f is nonzero if the amplitude of changing rate ζ is higher than a threshold. Equation (10) shows that the failure-rate is given by the losing rate of physical balances.

Then, from (8) and (10), it can be seen that operation reliability R can be evaluated online by the real-time estimation of disturbance changing rate ζ . Actually, the estimation of total disturbance ξ and its changing rate ζ plays a central role of online reliability assessment for energy systems, which leads to the following Problem.

Problem. Consider nonlinear system (1) describing energy system dynamics, where the condition of bounded disturbance changing-rate given by (4) and (5) as well as dissipation condition (6) are satisfied. How to provide a globally asymptotically bounded estimation of total disturbance ξ and its changing rate ζ .

3. Operation reliability assessment based on high-order extended state observer

In this section, a high order extended state-observer (HO-ESO) is newly proposed for the nonlinear system (1) satisfying conditions (4)–(7) so as to give a globally bounded estimation of the extended state-vector defined by

$$\mathbf{x} = [\mathbf{x}^T \quad \xi^T \quad \zeta^T]^T, \quad (12)$$

which is a solution of the Problem raised in the end of Section 2. Then the online reliability assessment can be given based on the estimations of the estimation of total disturbance and its changing rate. The design and performance analysis of this HO-ESO for online-reliability evaluation is

summarized as the following Theorem, which is the main result of this paper.

Theorem(HO-ESO). For nonlinear system (1) satisfying conditions (4), (5) and (6), design the HO-ESO as

$$\begin{cases} \dot{\hat{\mathbf{y}}} = \mathbf{f}_o(\hat{\mathbf{y}}, \hat{\mathbf{z}}) + \mathbf{G}(\mathbf{y})\mathbf{u} + \hat{\xi} - \varepsilon^{-1}\alpha_1 \mathbf{e}_y \\ \dot{\hat{\mathbf{z}}} = \mathbf{f}_i(\hat{\mathbf{y}}, \hat{\mathbf{z}}) \\ \dot{\hat{\xi}} = -\varepsilon^{-2}\alpha_2 \mathbf{e}_y + \hat{\zeta} \\ \dot{\hat{\zeta}} = -\varepsilon^{-3}\alpha_3 \mathbf{e}_y \end{cases} \quad (13)$$

where $\hat{\mathbf{y}}$, $\hat{\mathbf{z}}$, $\hat{\xi}$ and $\hat{\zeta}$ are respectively the estimations of \mathbf{y} , \mathbf{z} , ξ and ζ , $\mathbf{e}_y = \hat{\mathbf{y}} - \mathbf{y}$, and both ε and α_i ($i = 1, 2, 3$) are positive constants. HO-ESO (13) can provide globally bounded estimations of state-vector \mathbf{x} , total disturbance ξ and its rate of change ζ if the following conditions are well satisfied:

(A) Algebraic equation

$$s^3 + \alpha_1 s^2 + \alpha_2 s + \alpha_3 = 0 \quad (14)$$

is Hurwitz, i.e. all the roots of (14) has a strictly negative real parts.

(B) Storage function S satisfies

$$\frac{\partial^2 S(\mathbf{x})}{\partial \mathbf{y}^2} = \mathbf{T}(\mathbf{y}) \quad (15)$$

with $\mathbf{T}(\cdot)$ being positive-definite.

Proof: The observation errors related to measurable state-vector \mathbf{y} , unmeasurable state-vector \mathbf{z} , total disturbance ξ and its rate of change ζ are given by

$$\mathbf{e}_y = \hat{\mathbf{y}} - \mathbf{y} = [e_{y,1} \quad \dots \quad e_{y,m}]^T \quad (16)$$

$$\mathbf{e}_z = \hat{\mathbf{z}} - \mathbf{z} = [e_{z,1} \quad \dots \quad e_{z,n-m}]^T \quad (17)$$

$$\mathbf{e}_\xi = \hat{\xi} - \xi = [e_{\xi,1} \quad \dots \quad e_{\xi,m}]^T \quad (18)$$

and

$$\mathbf{e}_\zeta = \hat{\zeta} - \zeta = [e_{\zeta,1} \quad \dots \quad e_{\zeta,m}]^T \quad (19)$$

respectively. From (1), (4) and (13), the observation error dynamics satisfies

$$\begin{cases} \dot{\mathbf{e}}_y = \dot{\hat{\mathbf{y}}} - \dot{\mathbf{y}} = \mathbf{f}_o(\hat{\mathbf{y}}, \hat{\mathbf{z}}) - \mathbf{f}_o(\mathbf{y}, \hat{\mathbf{z}}) + \mathbf{e}_\xi - \varepsilon^{-1}\alpha_1 \mathbf{e}_y, \\ \dot{\mathbf{e}}_z = \dot{\hat{\mathbf{z}}} - \dot{\mathbf{z}} = \mathbf{f}_i(\hat{\mathbf{y}}, \hat{\mathbf{z}}) - \mathbf{f}_i(\mathbf{y}, \hat{\mathbf{z}}), \\ \dot{\mathbf{e}}_\xi = \dot{\hat{\xi}} - \dot{\xi} = -\varepsilon^{-2}\alpha_2 \mathbf{e}_y + \mathbf{e}_\zeta, \\ \dot{\mathbf{e}}_\zeta = \dot{\hat{\zeta}} - \dot{\zeta} = -\varepsilon^{-3}\alpha_3 \mathbf{e}_y - \mathbf{d}. \end{cases} \quad (20)$$

Based on the Taylor expansion of functions f_o and f_i around e_x defined by

$$\mathbf{e}_x = [\mathbf{e}_y \quad \mathbf{e}_z]^T, \quad (21)$$

it can be seen that

$$\mathbf{f}_a(\hat{\mathbf{x}}) = \mathbf{f}_a(\mathbf{e}_x + \mathbf{x}) = \mathbf{f}_a(\mathbf{e}_x) + \mathbf{h}_a(\mathbf{e}_x, \mathbf{x}), \quad a = o, i. \quad (22)$$

Since f_o and f_i are norm-bounded, it can be seen from (22) that both functions h_o and h_i are norm-bounded. Then, observation error dynamics (20) can be rewritten as

$$\begin{cases} \dot{\mathbf{e}}_y = \mathbf{f}_o(\mathbf{e}_x) + \mathbf{h}_o(\mathbf{e}_x, \mathbf{x}) + \mathbf{e}_\xi - \varepsilon^{-1}\alpha_1 \mathbf{e}_y, \\ \dot{\mathbf{e}}_z = \mathbf{f}_i(\mathbf{e}_x) + \mathbf{h}_i(\mathbf{e}_x, \mathbf{x}), \\ \dot{\mathbf{e}}_\xi = -\varepsilon^{-2}\alpha_2 \mathbf{e}_y + \mathbf{e}_\zeta, \\ \dot{\mathbf{e}}_\zeta = -\varepsilon^{-3}\alpha_3 \mathbf{e}_y - \mathbf{d}. \end{cases} \quad (23)$$

Moreover, under the scale transformation given by

$$\tau = t/\varepsilon, \quad (24)$$

and the coordinate transformation given by

$$\begin{cases} \bar{\mathbf{e}}_\xi = \varepsilon \mathbf{e}_\xi, \\ \bar{\mathbf{e}}_\zeta = \varepsilon^2 \mathbf{e}_\zeta, \end{cases} \quad (25)$$

observation error dynamics (23) can be further expressed as

$$\frac{d}{d\tau} \begin{bmatrix} \mathbf{e}_y \\ \mathbf{e}_z \\ \bar{\mathbf{e}}_\xi \\ \bar{\mathbf{e}}_\zeta \end{bmatrix} = \begin{bmatrix} \varepsilon [\mathbf{f}_o(\mathbf{e}_x) + \mathbf{h}_o(\mathbf{e}_x, \mathbf{x})] + \bar{\mathbf{e}}_\xi - \alpha_1 \mathbf{e}_y \\ \varepsilon [\mathbf{f}_i(\mathbf{e}_x) + \mathbf{h}_i(\mathbf{e}_x, \mathbf{x})] \\ -\alpha_2 \mathbf{e}_y + \bar{\mathbf{e}}_\zeta \\ -\alpha_3 \mathbf{e}_y - \varepsilon^2 \mathbf{d} \end{bmatrix}. \quad (26)$$

Choose the Lyapunov function of error dynamics (26) as

$$V(\mathbf{e}) = S(\mathbf{e}_x) + \frac{1}{2} \sum_{k=1}^m \bar{\mathbf{e}}_k^T \mathbf{P} \bar{\mathbf{e}}_k, \quad (27)$$

where

$$\mathbf{e} = [\mathbf{e}_x^T \quad \mathbf{e}_\xi^T \quad \mathbf{e}_\zeta^T]^T \quad (28)$$

$$\bar{\mathbf{e}}_k = [e_{y,k} \quad \varepsilon e_{\xi,k} \quad \varepsilon^2 e_{\zeta,k}]^T, \quad k = 1, \dots, m, \quad (29)$$

$e_{y,k}$, $e_{\xi,k}$ and $e_{\zeta,k}$ are respectively the k th element of \mathbf{e}_y , \mathbf{e}_ξ and \mathbf{e}_ζ . Further, define

$$\bar{\mathbf{e}} = [\bar{\mathbf{e}}_1^T \quad \bar{\mathbf{e}}_2^T \quad \dots \quad \bar{\mathbf{e}}_m^T]^T = [[e_{y,1} \quad \varepsilon e_{\xi,1} \quad \varepsilon^2 e_{\zeta,1}] \quad [e_{y,2} \quad \varepsilon e_{\xi,2} \quad \varepsilon^2 e_{\zeta,2}] \quad \dots \quad [e_{y,m} \quad \varepsilon e_{\xi,m} \quad \varepsilon^2 e_{\zeta,m}]]^T, \quad (30)$$

$$\bar{\mathbf{e}}_y = [\bar{\mathbf{e}}_y^T \quad \bar{\mathbf{e}}_\xi^T \quad \bar{\mathbf{e}}_\zeta^T]^T = [[e_{y,1} \dots e_{y,m}] \quad [\varepsilon e_{\xi,1} \dots \varepsilon e_{\xi,m}] \quad [\varepsilon^2 e_{\zeta,1} \dots \varepsilon^2 e_{\zeta,m}]]^T, \quad (31)$$

It can be seen from equations (30) and (31) that vector $\bar{\mathbf{e}}$ can be obtained from vector $\bar{\mathbf{e}}_y$ by reordering the entries, which can be given as the transformation satisfying

$$\bar{\mathbf{e}} = \mathbf{U} \bar{\mathbf{e}}_y \quad (32)$$

where matrix \mathbf{U} denotes the operation of reordering, and is given by

$$\mathbf{U} = \begin{bmatrix} \mathbf{U}_1 \\ \vdots \\ \mathbf{U}_m \end{bmatrix}; \quad (33)$$

$$\mathbf{U}_k = \mathbf{I}_3 \otimes \mathbf{v}_k = \begin{bmatrix} \mathbf{v}_k & \mathbf{O}_{1 \times m} & \mathbf{O}_{1 \times m} \\ \mathbf{O}_{1 \times m} & \mathbf{v}_k & \mathbf{O}_{1 \times m} \\ \mathbf{O}_{1 \times m} & \mathbf{O}_{1 \times m} & \mathbf{v}_k \end{bmatrix}, \quad k = 1, \dots, m, \quad (34)$$

$$\mathbf{v}_k = [v_{k,i}]_{1 \times m}, \quad v_{k,i} = \begin{cases} 1, & i = k, \\ 0, & i \neq k, \end{cases} \quad i = 1, \dots, m, \quad (35)$$

and \otimes is the Kronecker product operation between matrices or vectors. From equations (34) and (35), we can further obtain that

$$\begin{aligned} \frac{dV(\mathbf{e})}{d\tau} &= \frac{dS(\mathbf{e}_x)}{d\tau} + \bar{\mathbf{e}}_y^T \mathbf{U}^T \bar{\mathbf{P}} \mathbf{U} \frac{d\bar{\mathbf{e}}_y}{d\tau} \\ &= \frac{dS(\mathbf{e}_x)}{d\tau} + \bar{\mathbf{e}}^T \bar{\mathbf{P}} (\mathbf{U} \bar{\mathbf{A}} \mathbf{U}^T) \bar{\mathbf{e}} + \varepsilon \bar{\mathbf{e}}_y^T \mathbf{U}^T \bar{\mathbf{P}} \mathbf{U} \boldsymbol{\eta}(\mathbf{x}, \mathbf{e}_x, \mathbf{d}) \\ &= \frac{dS(\mathbf{e}_x)}{d\tau} + \bar{\mathbf{e}}^T \bar{\mathbf{P}} (\mathbf{I}_m \otimes \mathbf{A}) \bar{\mathbf{e}} + \varepsilon \bar{\mathbf{e}}_y^T \mathbf{U}^T \bar{\mathbf{P}} \mathbf{U} \boldsymbol{\eta}(\mathbf{x}, \mathbf{e}_x, \mathbf{d}) \\ &= \varepsilon \left[\frac{\partial S(\mathbf{e}_x)}{\partial \mathbf{e}_x} \right]^T [\mathbf{f}(\mathbf{e}_x) + \mathbf{h}(\mathbf{e}_x, \mathbf{x})] + \mathbf{s}^T(\mathbf{e}_y) [\bar{\mathbf{e}}_\xi - \alpha_1 \mathbf{e}_y] + \frac{1}{2} \sum_{k=1}^m \bar{\mathbf{e}}_k^T (\mathbf{A}^T \mathbf{P} + \mathbf{P} \mathbf{A}) \bar{\mathbf{e}}_k + \varepsilon \bar{\mathbf{e}}_y^T \mathbf{U}^T \bar{\mathbf{P}} \mathbf{U} \boldsymbol{\eta}(\mathbf{x}, \mathbf{e}_x, \mathbf{d}), \end{aligned} \quad (46)$$

$$\mathbf{U}_k \mathbf{U}_j^T = \begin{cases} \mathbf{I}_3, & k = j, \\ \mathbf{O}_3, & k \neq j, \end{cases} \quad (36)$$

and

$$\mathbf{U}_k^T \mathbf{U}_j = \begin{cases} \mathbf{I}_3 \otimes \mathbf{V}_k, & k = j, \\ \mathbf{O}, & k \neq j, \end{cases} \quad (37)$$

where

$$\mathbf{V}_k = \text{diag}(\mathbf{v}_k) = \begin{bmatrix} v_{k,1} & & \\ & \ddots & \\ & & v_{k,m} \end{bmatrix}. \quad (38)$$

Based on (36) and (37), we have

$$\mathbf{U}^T \mathbf{U} = \mathbf{U} \mathbf{U}^T = \mathbf{I}_{3m}, \quad (39)$$

which shows that \mathbf{U} is an orthogonal matrix. By applying the reordering transformation given by (32)–(35), Lyapunov function (27) can be rewritten as

$$V(\mathbf{e}) = S(\mathbf{e}_x) + \frac{1}{2} \bar{\mathbf{e}}^T \bar{\mathbf{P}} \bar{\mathbf{e}} = S(\mathbf{e}_x) + \frac{1}{2} \bar{\mathbf{e}}_y^T \mathbf{U}^T \bar{\mathbf{P}} \mathbf{U} \bar{\mathbf{e}}_y, \quad (40)$$

$$\bar{\mathbf{P}} = \mathbf{I}_m \otimes \mathbf{P} = \begin{bmatrix} \mathbf{P} & & \\ & \ddots & \\ & & \mathbf{P} \end{bmatrix}. \quad (41)$$

Moreover, from observation error dynamics (26), it can be seen that

$$\frac{d\bar{\mathbf{e}}_y}{d\tau} = \bar{\mathbf{A}} \bar{\mathbf{e}}_y + \varepsilon \boldsymbol{\eta}(\mathbf{x}, \mathbf{e}_x, \mathbf{d}), \quad (42)$$

where

$$\bar{\mathbf{A}} = \begin{bmatrix} -\alpha_1 \mathbf{I}_m & \mathbf{I}_m & \mathbf{O}_m \\ -\alpha_2 \mathbf{I}_m & \mathbf{O}_m & \mathbf{I}_m \\ -\alpha_3 \mathbf{I}_m & \mathbf{O}_m & \mathbf{O}_m \end{bmatrix} = \mathbf{A} \otimes \mathbf{I}_m, \quad (43)$$

$$\mathbf{A} = \begin{bmatrix} -\alpha_1 & 1 & 0 \\ -\alpha_2 & 0 & 1 \\ -\alpha_3 & 0 & 0 \end{bmatrix}, \quad (44)$$

$$\boldsymbol{\eta}(\mathbf{x}, \mathbf{e}_x, \mathbf{d}) = \begin{bmatrix} \mathbf{f}_o(\mathbf{e}_x) + \mathbf{h}_o(\mathbf{e}_x, \mathbf{x}) \\ \mathbf{O} \\ -\varepsilon^2 \mathbf{d} \end{bmatrix}, \quad (45)$$

Then, differentiate function V along the trajectory of (26),

where

$$\mathbf{h}(\mathbf{e}_x, \mathbf{x}) = \begin{bmatrix} \mathbf{h}_o(\mathbf{e}_x, \mathbf{x}) \\ \mathbf{h}_i(\mathbf{e}_x, \mathbf{x}) \end{bmatrix}, \quad (47)$$

$$\mathbf{s}(\mathbf{e}_y) = \frac{\partial S(\mathbf{e}_x)}{\partial \mathbf{e}_y}. \quad (48)$$

Since algebraic equation (14) is Hurwitz, for arbitrary positive-definite matrix \mathbf{Q} , there exists positive-definite matrix \mathbf{P} so that

$$\mathbf{A}^T \mathbf{P} + \mathbf{P} \mathbf{A} = -\mathbf{Q}. \quad (49)$$

Moreover, from conditions (48) and (15),

$$\mathbf{s}(\mathbf{e}_y) = \mathbf{T}(\mathbf{e}_y) \mathbf{e}_y + \mathbf{o}(\|\mathbf{e}_y\|_2), \quad (50)$$

which further shows that

$$\begin{cases} \mathbf{s}^T(\mathbf{e}_y) \mathbf{e}_y = \gamma \|\mathbf{e}_y\|_2^2, \\ \|\mathbf{s}(\mathbf{e}_y)\|_2^2 = \theta \|\mathbf{e}_y\|_2^2, \end{cases} \quad (51)$$

where γ and θ are some positive constants, and $\mathbf{o}(\cdot)$ denotes the high order terms. Substitute (49), (50) and (51) to (46),

$$\frac{dV}{dt} \leq -\varepsilon Q(\mathbf{e}_x) - \frac{1}{4\varepsilon} \bar{\mathbf{e}}_y^T \mathbf{U}^T \bar{\mathbf{Q}} \mathbf{U} \bar{\mathbf{e}}_y - \frac{\alpha_1 \gamma}{2} \|\mathbf{e}_y\|_2^2 + \frac{\varepsilon^2 \theta^2}{2\alpha_1 \gamma} \|\mathbf{e}_\xi\|_2^2 + \varepsilon^2 \mathbf{\eta}^T(\mathbf{e}_x, \mathbf{d}) \mathbf{U} \bar{\mathbf{P}}^T \bar{\mathbf{Q}}^{-1} \bar{\mathbf{P}} \mathbf{U} \mathbf{\eta}(\mathbf{e}_x, \mathbf{d}), \quad (52)$$

where

$$\bar{\mathbf{Q}} = \mathbf{I}_m \otimes \mathbf{Q}. \quad (53)$$

From scaling transformation (24) and inequality (52)

$$\frac{dV}{dt} \leq -Q(\mathbf{e}_x) - \frac{1}{4\varepsilon} \bar{\mathbf{e}}_y^T \mathbf{U}^T \bar{\mathbf{Q}} \mathbf{U} \bar{\mathbf{e}}_y - \frac{\alpha_1 \gamma}{2\varepsilon} \|\mathbf{e}_y\|_2^2 + \frac{\varepsilon \theta^2}{2\alpha_1 \gamma} \|\mathbf{e}_\xi\|_2^2 + \varepsilon \mathbf{\eta}^T(\mathbf{e}_x, \mathbf{d}) \mathbf{U} \bar{\mathbf{P}}^T \bar{\mathbf{Q}}^{-1} \bar{\mathbf{P}} \mathbf{U} \mathbf{\eta}(\mathbf{e}_x, \mathbf{d}), \quad (54)$$

which means that the estimation error converge globally asymptotically to a bounded neighborhood around the origin, and a smaller scaling factor can give a smaller steady error and a faster convergence. This completes the Proof.

Remark 1. Usually, it is easy to choose positive constants α_i ($i = 1, 2, 3$) so that condition (A) can be satisfied. The difficulty in applying ESO (13) is to check dissipation condition (6) and condition (B) given by (48) and (15). For mechanical, electrical and electromechanical systems, total energy can be adopted as the storage function.

Remark 2. (Online Reliability Estimator). From (8), (13) and (10), the operational reliability can be estimated by

$$\hat{R}(t) = \exp \left[- \int_0^t \hat{r}_f(\tau) d\tau \right] = \exp \left\{ - \int_0^t \left[\sum_{k=1}^m |dz(\hat{\zeta}_k(\tau), b_k, l_k)| \right] d\tau \right\}, \quad (55)$$

where $\hat{\zeta}_k$ ($k = 1, \dots, m$) is given by the HO-ESO (13) with observer gains satisfying conditions (A) and (B) in Theorem (HO-ESO).

Remark 3. There main differences between the HO-ESO and the

classical extended state-observer (ESO) mainly lie in the following two aspects: First, the HO-ESO is applicable to nonlinear dissipative system (1) satisfying properties (6) and (15), while the ESO is mainly given for the dynamic systems in the following strict feedback form

$$\begin{cases} \dot{x}_{k,i} = x_{k,i+1}, & i = 1, \dots, n_k - 1, \\ x_{k,n_k} = v_k, & k = 1, \dots, r, \end{cases} \quad (56)$$

where

$$\mathbf{x} = \begin{bmatrix} \mathbf{x}_1 \\ \vdots \\ \mathbf{x}_r \end{bmatrix}, \quad \mathbf{x}_k = \begin{bmatrix} x_{k,1} \\ \vdots \\ x_{k,n_k} \end{bmatrix} \quad (k = 1, \dots, r) \quad (57)$$

is state-vector of system (56), and

$$\xi = [\xi_1 \ \dots \ \xi_r]^T \quad (58)$$

is the total disturbance of system (56). If the system dynamics does not take the form as (56), then the operation of feedback linearization should be first applied to transform the system into strict feedback form (56) by injecting extra linearization control input. Second, the classical ESO gives the observation of total disturbance ξ , while the HO-ESO gives the observations of both total disturbance ξ and its rate of change $\dot{\xi}$.

4. Application to pressurized water reactors

In this section, HO-ESO (13) and reliability estimator (55) is applied to evaluate the operation reliability of pressurized water reactors (PWRs). Based on giving the dynamic model, both dissipation condition (6) and condition (B) given by (48) and (15) are verified, and the

expression of a special HO-ESO for PWRs is given.

4.1. State-space model of PWR dynamics

The PWR dynamic model for ESO design is the point kinetics with one equivalent delayed neutron group and temperature feedback from both the fuel and coolant temperature, which is given as follows [49,50]:

$$\begin{cases} \dot{n}_r = -\frac{\beta}{\Lambda} (n_r - c_r) + \frac{n_r \rho_r}{\Lambda} + \frac{n_r}{\Lambda} [\alpha_f (T_f - T_{f,m}) + \alpha_c (T_{cav} - T_{cav,m})], \\ \dot{c}_r = \lambda (n_r - c_r), \\ \dot{T}_f = \frac{1}{\mu_f} [\gamma_f P_0 n_r - \Omega (T_f - T_{cav})], \\ \dot{T}_{cav} = \frac{1}{\mu_c} [(1 - \gamma_f) P_0 n_r + \Omega (T_f - T_{cav}) - 2M (T_{cav} - T_{cin})], \end{cases} \quad (59)$$

where n_r and c_r are respectively the normalized neutron flux and concentration of delayed neutron precursor, β is the fraction of delayed neutrons, Λ is the effective lifetime of prompt neutron, λ is the decay constant of delayed neutron precursor, T_f is the average fuel

temperature, T_{cav} and T_{cin} are the average and inlet primary coolant temperatures respectively, $T_{f,m}$ and $T_{\text{cav},m}$ are the initial equilibrium values corresponding to T_f and T_{cav} respectively, α_f and α_c are the reactivity feedback coefficients of the fuel and coolant temperatures respectively, Ω is the heat transfer coefficient between fuel and coolant, M is the mass flow rate times heat capacity of the primary coolant, P_0 is the rated thermal power, ρ_r is the exterior reactivity, μ_f is the total heat capacity of fuel, μ_c is the total heat capacity of primary coolant, γ_f is the fraction of reactor power deposited in the fuel, and $0 < \gamma_f < 1$. Here, it is not loss of generality to suppose that both α_f and α_c are strictly negative.

Define the state-vector x , measurement output y and total disturbance ξ of PWR dynamics as

$$\begin{cases} \mathbf{x} = [x_i]_{1 \times 4} = [n_r \ T_{\text{cav}} \ c_r \ T_f]^T, \\ \mathbf{y} = \mathbf{Cx}, \\ \boldsymbol{\xi} = [\Lambda^{-1} n_r \delta \rho_r \ 2\mu_c^{-1} M T_{\text{cin}}]^T, \end{cases} \quad (60)$$

where

$$\mathbf{C} = [\mathbf{I}_2 \ \mathbf{O}_2], \quad (61)$$

$$\delta \rho_r = \rho_r - \alpha_f T_{f,m} - \alpha_c T_{\text{cav},m}. \quad (62)$$

Then, the state-space model of PWRs can be written as

$$\dot{\mathbf{x}} = \mathbf{f}(\mathbf{x}) + \mathbf{C}^T \boldsymbol{\xi}, \quad (63)$$

where

$$\mathbf{f}(\mathbf{x}) = \begin{bmatrix} -\frac{\beta}{\Lambda} (x_1 - x_3) + \frac{1}{\Lambda} (n_{r0} + x_1) (\alpha_c x_2 + \alpha_f x_4) \\ \frac{P_0}{\mu_c} (1 - \gamma_f) x_1 - \frac{\Omega}{\mu_c} (x_2 - x_4) - \frac{2M}{\mu_c} x_2 \\ \lambda (x_1 - x_3) \\ \frac{P_0}{\mu_f} \gamma_f x_1 + \frac{\Omega}{\mu_f} (x_2 - x_4) \end{bmatrix}. \quad (64)$$

4.2. Verification of dissipativity

To apply HO-ESO (13) for online operational reliability analysis, it is central to verify that PWR dynamics (63) is strictly dissipative under a proper storage function. The verification of dissipativity is summarized as the following proposition.

Proposition (Dissipativity of PWR). The dynamics of PWR given by (63) with negative temperature reactivity feedback coefficients α_f and α_c is strictly dissipative under storage function S satisfying

$$S(\mathbf{x}) = \left[\Lambda x_1 + \frac{\beta}{\lambda} x_3 - n_{r0} \ln \left(1 + \frac{x_1}{n_{r0}} \right)^{\lambda} \left(1 + \frac{x_3}{n_{r0}} \right)^{\frac{\beta}{\lambda}} \right] - \frac{1}{2P_0} \left(\frac{\alpha_c \mu_c}{1 - \gamma_f} x_2^2 + \frac{\alpha_f \mu_f}{\gamma_f} x_4^2 \right), \quad (65)$$

if inequality

$$\left[1 - \frac{\alpha_c \gamma_f}{\alpha_f (1 - \gamma_f)} \right]^2 < \frac{8M \alpha_c \gamma_f}{\Omega \alpha_f (1 - \gamma_f)} \quad (66)$$

is well satisfied.

Proof: Since both temperature reactivity feedback coefficients α_f and α_c are guaranteed to be strictly negative by reactor physical design, it can be seen that storage function $S(x)$ defined by (65) is strictly positive definite. Moreover, if inequality (66) is satisfied, then there is a positive constant $\sigma \in (0, 1)$ so that

$$\left[1 - \frac{\alpha_c \gamma_f}{\alpha_f (1 - \gamma_f)} \right]^2 = \frac{8\sigma M \alpha_c \gamma_f}{\Omega \alpha_f (1 - \gamma_f)} \quad (67)$$

From dissipation condition (6), it can be derived that

$$\begin{aligned} \left(\frac{\partial S}{\partial \mathbf{x}} \right)^T \mathbf{f}(\mathbf{x}) &= -\frac{\beta(x_1 - x_3)^2}{(n_{r0} + x_1)(n_{r0} + x_3)} \\ &+ \frac{\alpha_f \Omega}{\gamma_f P_0} \left[x_4^2 - x_2 x_4 - \frac{\gamma_f}{1 - \gamma_f} \cdot \frac{\alpha_c}{\alpha_f} \left(\left(1 + \frac{2M}{\Omega} \right) x_4^2 - x_2 x_4 \right) \right]. \end{aligned} \quad (68)$$

From equations (67) and (68), dissipation condition (6) is satisfied with positive-definite function Q given by

$$Q(\mathbf{x}) = \frac{\beta(x_1 - x_3)^2}{(n_{r0} + x_1)(n_{r0} + x_3)} - \frac{2(1 - \sigma) \alpha_c M}{(1 - \gamma_f) P_0} x_4^2 - \frac{\alpha_f \Omega}{\gamma_f P_0} \left[x_4 - \frac{1}{2} \left(1 + \frac{\gamma_f}{1 - \gamma_f} \cdot \frac{\alpha_c}{\alpha_f} \right) x_2 \right]^2 > 0, \quad (69)$$

which completes the Proof of this proposition.

Remark 4. From equation (65), it can be verified that

$$\mathbf{s}(\mathbf{y}) = \frac{\partial S(\mathbf{x})}{\partial \mathbf{y}} = \begin{bmatrix} \Lambda x_1 & \frac{\alpha_c \mu_c}{(1 - \gamma_f) P_0} x_2 \end{bmatrix}^T, \quad (70)$$

$$\frac{\partial^2 S(\mathbf{x})}{\partial \mathbf{y}^2} = \text{diag} \left(\begin{bmatrix} \frac{\Lambda n_{r0}}{(n_{r0} + x_1)^2} & \frac{\alpha_c \mu_c}{(1 - \gamma_f) P_0} \end{bmatrix} \right) = \mathbf{T}(x_1) > 0. \quad (71)$$

From (70), (71) and the proposition, it can be seen that ESO can be applied to PWRs satisfying (66) for online reliability estimation.

4.3. HO-ESO for PWRs

From state-space model of PWRs (63), it can be seen that $m = 2$, and then based on the Theorem proposed in Section 2, the HO-ESO of PWRs can be designed as

$$\begin{cases} \dot{\hat{x}}_1 = \mathbf{f}(\hat{\mathbf{x}}) + \mathbf{C}^T [\hat{\boldsymbol{\xi}} - \varepsilon^{-1} \alpha_1 \mathbf{e}_y], \\ \dot{\hat{x}}_2 = -\varepsilon^{-2} \alpha_2 \mathbf{e}_y + \hat{\boldsymbol{\zeta}}, \\ \dot{\hat{\boldsymbol{\zeta}}} = -\varepsilon^{-3} \alpha_3 \mathbf{e}_y, \end{cases} \quad (72)$$

where

$$\mathbf{e}_y = [\hat{x}_1 - x_1 \ \hat{x}_2 - x_2]^T. \quad (73)$$

$\hat{\boldsymbol{\xi}}, \hat{\boldsymbol{\zeta}} \in \mathbb{R}^2$, function f is given by equation (64), and positive constants $\alpha_i (i = 1, 2, 3)$ satisfy condition (A) in the Theorem. Since condition (B) is guaranteed by the above proposition, observer (72) can provide a

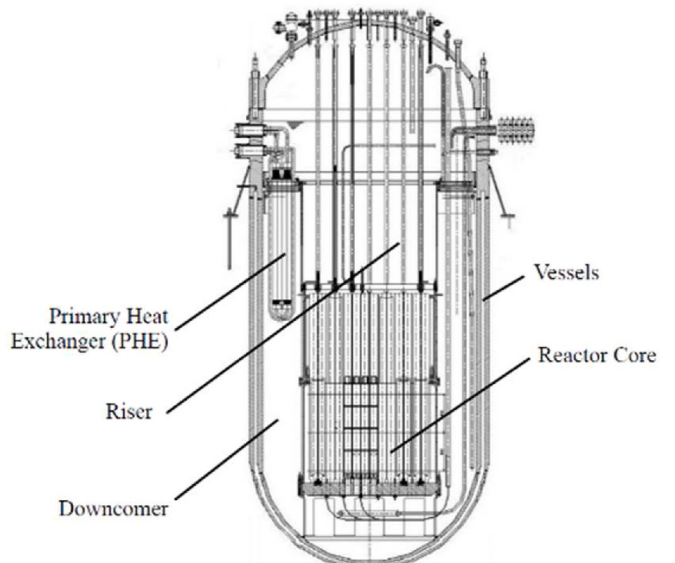


Fig. 1. The schematic diagram of NHR.

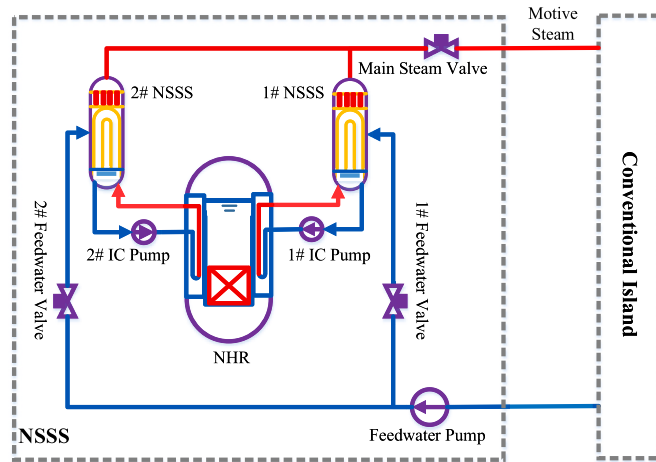


Fig. 2. The simplified process diagram of NHR-based nuclear steam supply system.

globally asymptotically bounded estimation.

5. Simulation results with discussions

In this section, the HO-ESO of PWRs given by (72) is applied to the online operation reliability estimation of a nuclear heating reactor (NHR) that is a typical integral pressurized water reactor (iPWR) developed by the institute of nuclear and new energy technology (INET) of Tsinghua University [51,52]. The NHR has a series of advanced features such as the integral primary circuit, full-power-range natural circulation, self-pressure, passive removal of residual heat and hydraulically control rod driving [52,53]. The schematic diagram of NHR with a rated thermal power of 200MW_{th} is shown in Fig. 1, and corresponding simplified process diagram of NHR-based nuclear supplying system (NSSS) is shown in Fig. 2, where the conventional island

can be a turbine-generator system, a district heating system, a seawater desalination system or their combinations. The cold water leaving from the primary side of primary heat exchangers (PHEs) enters to the reactor core from its bottom, which is then heated up by the fission power. The output hot water flows upward along the riser, and enters to the primary sides of PHEs so as to transfer its heat to the secondary coolant. The primary circulation is naturally driven by coolant density difference. The secondary coolant flows of PHEs combine together to form two intermittent circuits (ICs) each of which drives a U-tube steam generator (UTSG) for power generation or heat supply.

5.1. Simulation results

In this numerical simulation, ESO (72) is applied to estimate the unmeasurable states and disturbances so as to evaluate its operation reliability of NHR online by equation (55). The parameters of ESO are chosen as $\alpha_1 = 3a$, $\alpha_2 = 3a^2$, $\alpha_3 = a^3$, and $a = 0.1$. Moreover, different values of parameter ε are adopted in the simulation. The reactor power controller and the UTSG water-level controller adopt the control strategies proposed in Refs. [54,55] respectively. To verify the feasibility and to show the performance, the simulation results in the following cases are given.

A. Normal Power Decrease

The NHR plant operates steadily at 100% full power (FP) initially. The setpoint of reactor thermal power is set to decrease at 3000s from 100%FP to 20%FP with a constant rate of 10%FP/min. The plant control system drives the control rods, IC pumps and UTSG feedwater valves so as to suppress the errors between the actual and reference values of the process variables. The dynamic responses of normalized neutron flux n_r , normalized precursor concentration c_r , averaged temperatures of fuel assembly T_f and primary coolant T_{cav} , are shown in Fig. 3. The estimations of both ξ_i and their differentiations ζ_i ($i = 1, 2$) are shown in Fig. 4.

After keeping running steadily at 100%FP for 3000s, a step decrease of reactivity with an amount of 0.3\$ is injected. The step decrease of

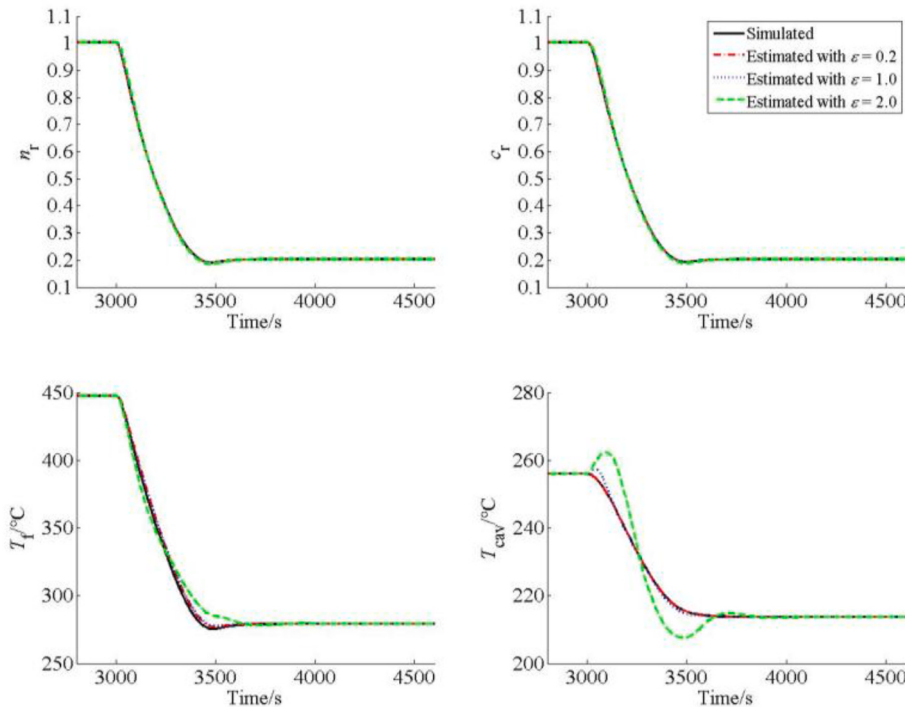


Fig. 3. Reponses of: normalized neutron flux n_r , precursor concentration c_r , averaged fuel temperature T_f , and averaged temperature of primary coolant T_{cav} in Case A.

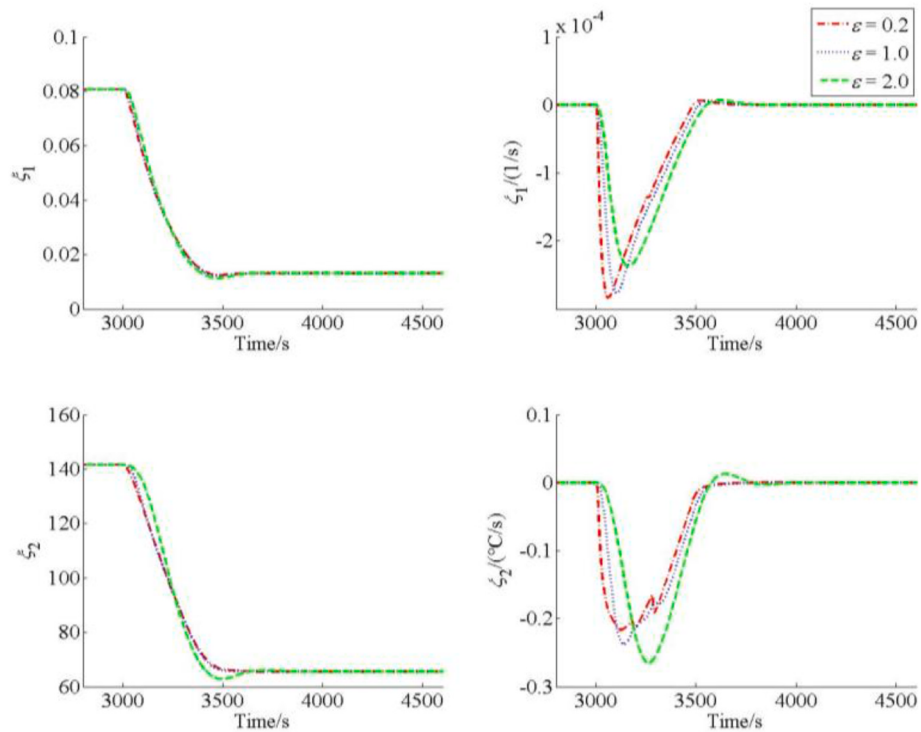


Fig. 4. Estimation of disturbances ξ_i and their differentiations ζ_i ($i = 1, 2$) in Case A.

B. Step Decrease of Reactivity

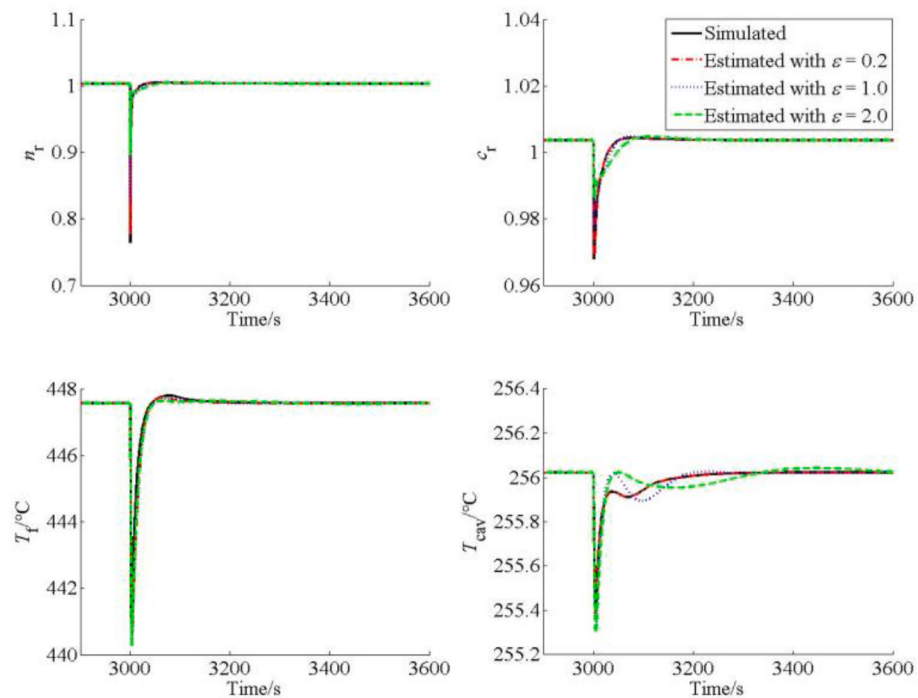


Fig. 5. Responses of normalized neutron flux n_r , precursor concentration c_r , averaged fuel temperature T_f , and averaged temperature of primary coolant T_{cav} in Case B.

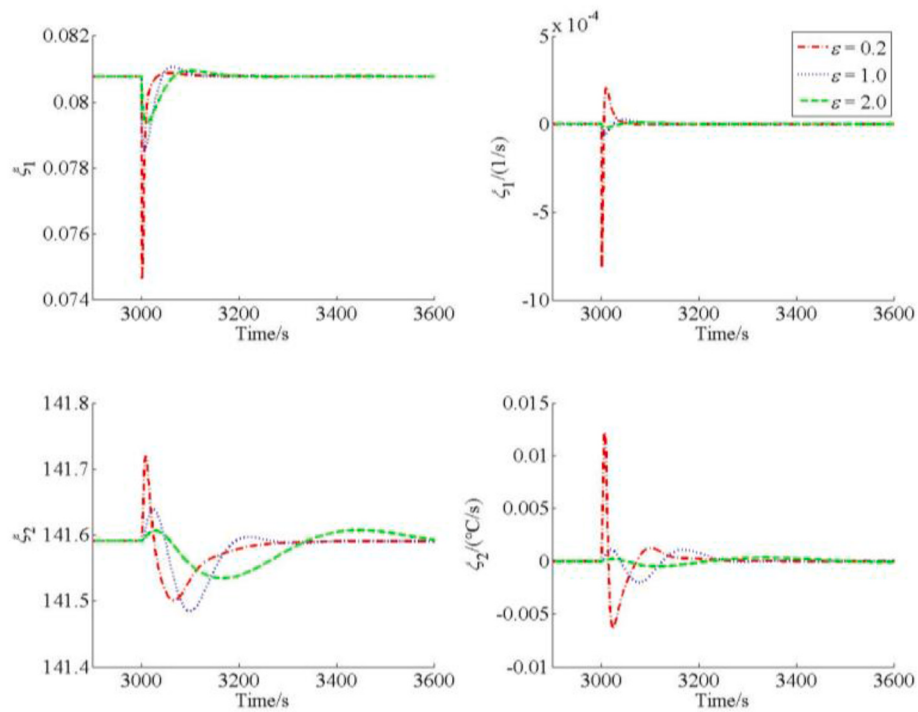


Fig. 6. Estimation of disturbances ξ_i and their differentiations ζ_i ($i = 1, 2$) in Case B.

C. Load Rejection

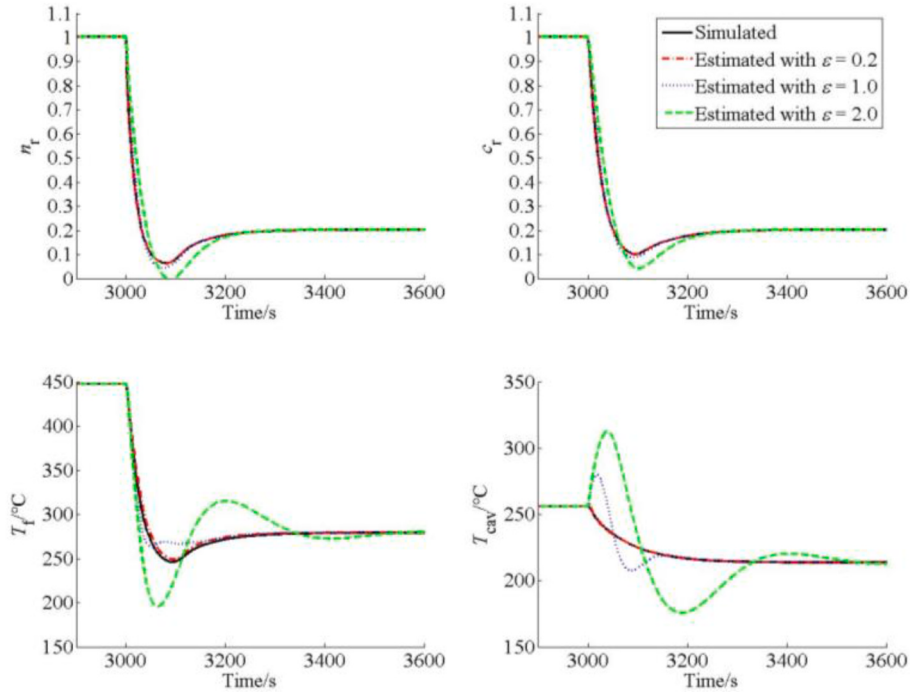


Fig. 7. Responses of: normalized neutron flux n_r , precursor concentration c_r , averaged fuel temperature T_f , and averaged temperature of primary coolant T_{cav} in Case C.

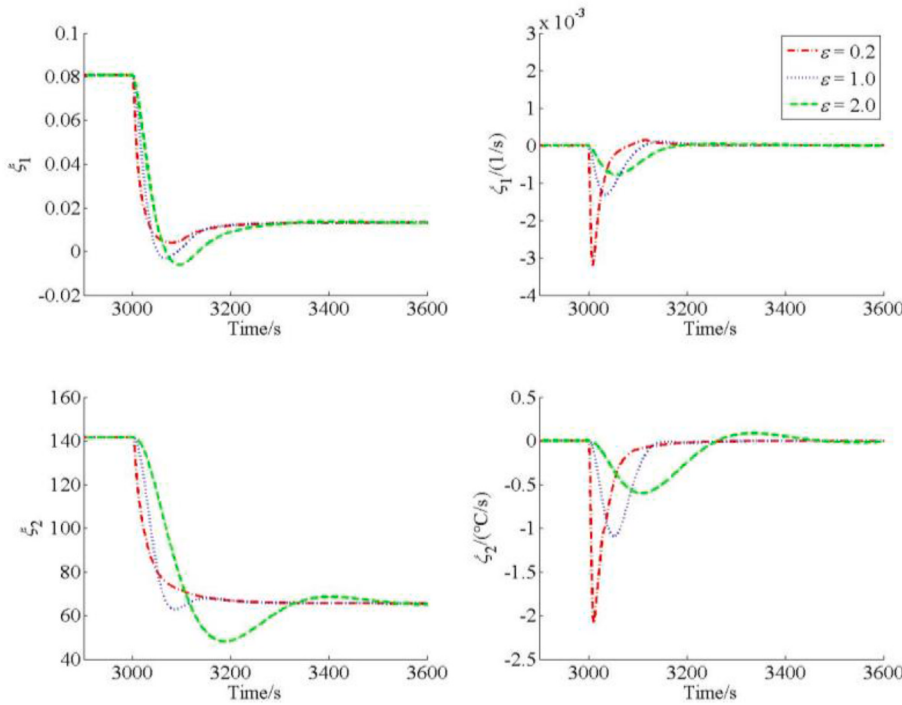


Fig. 8. Estimation of disturbances ξ_i and their differentiations ζ_i ($i = 1, 2$) in Case C.

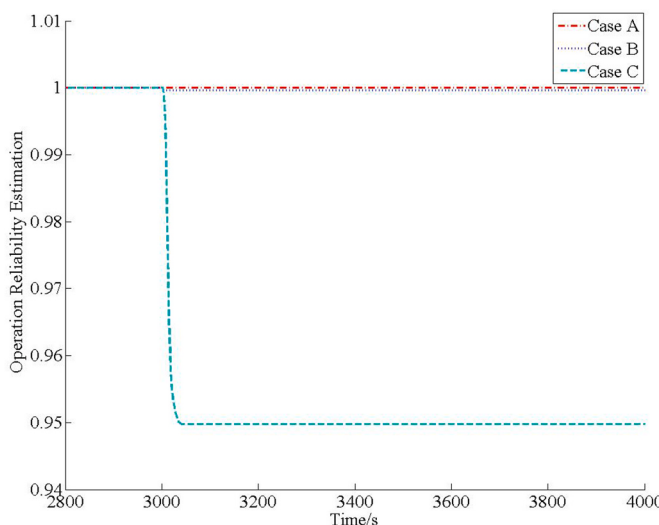


Fig. 9. Deterioration of reactor operation reliability in cases A, B and C.

reactivity leads to the errors of neutron flux and coolant temperature, which drives the control system to suppress the deviations of process variables by adjusting the speed of control rods, the rotation-rate of IC pumps and the openings of feedwater valves. The responses of process variables including the normalized neutron flux, normalized precursor concentration, averaged temperatures of fuel and primary coolant are all shown in Fig. 5, and the estimations of disturbances ξ_i and their differentiations ζ_i ($i = 1, 2$) are given in Fig. 6.

The load rejection is one of the most stressed condition of nuclear plant operation, which may be triggered by the trip of steam turbine. Initially, the NHR plant operates steadily at 100%FP, and then the set-point of reactor thermal power steps down directly from 100%FP to 20%FP. Due to the sudden step decrease of power setpoint, the errors of process variables such as the neutron flux, temperatures of fuel and coolant as well as coolant flowrates are enlarged abruptly, which drives

the control system to generate proper driving signals of control rods, IC pumps and UTSG feedwater valves so as to suppress the errors. The responses of process variables are shown in Fig. 7, and the estimations of disturbances and their differentiations are given in Fig. 8.

Moreover, the deterioration curves of reactor operation reliability in the cases of normal power decrease, reactivity step decrease and load rejection are all shown in Fig. 9, where the estimation of reliability is calculated based on (55) with the parameters of failure-rates given by (10) being chosen as $b_1 = 0.0005$, $b_2 = 1.5$, $l_1 = 0.5$ and $l_2 = 0.005$. Here, positive constant ε is set to be $\varepsilon = 0.2$ during the online assessment of reactor operation reliability.

5.2. Discussions

From Figs. 3, 5 and 7, it can be seen that the newly-built HO-ESO of PWR given by (72) provides asymptotically convergent observation for both the measurable and unmeasurable state-variables in normal operation cases such as power decreasing as well as typical abnormal cases such as reactivity step decrease and load rejection. Although the observation performance deteriorates with the increase of positive constant ε , the observations of state-variables as well as the disturbances and their differentiation are generally acceptable. Based on the Theorem and the proposition in sections 3 and 4, the convergence of HO-ESO is guaranteed by both the dissipation feature of nuclear reactor dynamics and the Hurwitz property of algebraic equation (14). However, from Figs. 4, 6 and 8, the transients of the estimations of disturbances ξ_i and their differentiations ζ_i ($i = 1, 2$) are sensitive to the value of positive constant ε . It can be further seen that the overshoots of $\hat{\xi}_1$ and $\hat{\zeta}_2$ are larger and steeper if constant ε is smaller. Usually, due to both the reactor reactivity and thermal-hydraulic uncertainty vary with the operation condition, disturbances ξ_i may not be zero at all the steady states. While, due to the globally asymptotical convergence of HO-ESO (72), the disturbance varying rate ζ_i ($i = 1, 2$) should be zero at steady states, otherwise the estimation of disturbances cannot be bounded. Hence, the HO-ESO proposed in this paper can be adopted as a smart soft sensor for the disturbances in the channels of reactor neutron kinetics and thermal-hydraulics, and, to guarantee a satisfactorily high

sensitivity, the value of constant ε should be small enough.

Furthermore, from the reactor operation reliability deterioration in all the three cases shown in Fig. 9 and calculated by both equation (55) and the estimations given by HO-ESO (72), it can be seen that there exists reliability deterioration in the abnormal cases, which is given by the fact that both negative reactivity injection and load rejections can induce larger and steeper overshoots of $\hat{\zeta}_1$ and $\hat{\zeta}_2$ that surpass the threshold of deadzone function. Since the load rejection triggers fast and large-range variations of the process variables with a larger duration, the reliability decrease in the case of load rejection is much larger than that corresponding to the case of reactivity step decrease. Actually, the duration of disturbance is just the transition period of operation reliability response shown in Fig. 9. Hence, it can be also seen that the HO-ESO based operation reliability assessment method given by (13) and (55) can applied to measure not only the amount but also the duration of the disturbances related to operation anomaly.

Based on the above discussion, the HO-ESO-based operation reliability assessing method is feasible for the online evaluation of reliability of nuclear reactors. It is easy to implement HO-ESO (72) on the digital control systems of the energy systems as an operation reliability monitoring module, which means that the method proposed in this paper is deployable. Moreover, the HO-ESO-based online reliability assessing method can provide operation assistance function so as to maintain a high level of system reliability, which is not only meaningful to the operation safety and stability but also vital to the economic competitiveness.

6. Conclusions

The mismatch between the expected and actual responses of a given energy producing or consuming system can be adopted to estimate both the total disturbance and its differentiation that can be utilized for operational reliability evaluation. The mismatch of system responses is essentially determined by the total disturbance to the energy system dynamics, and the total disturbance and its changing rate are tightly related to the failure-rate. In this paper, a high order extended state-observer (HO-ESO) is newly proposed for the nonlinear dissipative system representing the dynamics of typical energy systems, which can provide globally bounded estimations for the key process variables as well as the total disturbance and its differentiation. Then, the evaluation of energy system operation reliability is given based on the estimation of failure-rate given by the estimation of the changing rate of total disturbance. To verify this HO-ESO-based online reliability assessment method, it is applied to the wildly deployed PWR plants. After checking the dissipativity of general PWR dynamics, numerical simulation results related to a nuclear heating reactor in the cases of normal power decrease, reactivity step decrease and load rejection are all given, and the reliability deterioration curve in these cases are also shown. The simulation results strongly show both the feasibility and satisfactory performance of the HO-ESO-based energy system reliability estimation method.

Credit author statement

Zhe Dong: Conceptualization, Methodology, Writing – original draft, Supervision. Bowen Li: Investigation, Validation. Junyi Li: Writing – review & editing, Validation. Xiaojin Huang: Funding acquisition. Zuoyi Zhang: Project administration.

Declaration of competing interest

The authors declare that they have no known competing financial interests or personal relationships that could have appeared to influence the work reported in this paper.

Acknowledgement

This work is jointly supported by National S&T Major Project of China (Grants No. ZX069), Natural Science Foundation of China (NSFC) (Grant No. 62173202), as well as the opening fund of State Key Laboratory of Nuclear Power Safety Monitoring Technology and Equipment.

References

- [1] Marqusee J, Jetket II D. Reliability of emergency and standby diesel generators: impact on energy resiliency solutions. *Appl Energy* 2020;268:114918.
- [2] Tsai C-H, Figueira-Acevedo A, Boese M, Li Y, Nihal Mohan, Okullo J, Heath B, Bakke J. Challenges of planning for high renewable futures: experience in the U.S. midcontinent electricity market. *Renew Sustain Energy Rev* 2020;131:109992.
- [3] Sutharsan T, Montalvao D, Chen YK, Wang W-C, Pisac C, Elemar H. A review on prognostics and health monitoring of proton exchange membrane fuel cell. *Renew Sustain Energy Rev* 2017;75:440–50.
- [4] Ren Y, Fan D, Feng Q, Wang Z, Sun B, Yang D. Agent-based restoration approach for reliability with load balancing on smart grids. *Appl Energy* 2019;249:46–57.
- [5] Afzali P, Keynia F, Rashidinejad M. A new model for reliability-centered maintenance prioritization of distribution feeders. *Energy* 2019;171:701–9.
- [6] Artigao E, Martín-Martínez S, Honrubia-Escribano A. Wind turbine reliability: a comprehensive review towards effective condition monitoring development. *Appl Energy* 2018;1569–83.
- [7] Lei Y, Li N, Guo L, Li N, Yan T, Lin J. Machinery health prognostics: a systematic review from data acquisition to RUL prediction. *Mech Syst Signal Process* 2018; 104:799–834.
- [8] Wang J. System integration, durability and reliability of fuel cells: challenges and solutions. *Appl Energy* 2017;189:460–79.
- [9] Triki-Lahiani A, Abdelghani AB-B, Slama-Belkhodja I. Fault detection and monitoring systems for photovoltaic installations: a review. *Renew Sustain Energy Rev* 2018;82:2680–92.
- [10] Hacke P, Lokanath S, Williams P, Vasan A, Sochor P, Tamizhmani G, Shinohara H, Kurtz S. A status review of photovoltaic power conversion equipment reliability, safety, and quality assurance protocols. *Renew Sustain Energy Rev* 2018;82: 1097–112.
- [11] Dai J, Das D, Ohadi M, Pecht M. Reliability risk mitigation of free air cooling through prognostics and health management. *Appl Energy* 2013;111:104–12.
- [12] Heylen E, Deconinck G, Van Herrem D. Review and classification of reliability indicators for power systems with a high share of renewable energy sources. *Renew Sustain Energy Rev* 2018;97:554–68.
- [13] Gandoman FH, Jaguemont J, Goutam S, Gopalakrishnan R, Firouz Y, Kalogiannis T, Omar N, Van Mierlo J. Concept of reliability and safety assessment of lithium-ion batteries in electric vehicles: basics, progress, and challenges. *Appl Energy* 2019;251:113343.
- [14] Guo Y, Sheng S, Phillips C, Keller J, Veers P, Williams L. A methodology for reliability assessment and prognosis of bearing axial cracking in wind turbine gearboxes. *Renew Sustain Energy Rev* 2020;127:109888.
- [15] Johnson SC, Papageorgiou DJ, Mallapragada DS, Deetjen TA, Rhodes JD, Webber ME. Evaluating rotational inertial as a component of grid reliability with high penetration of variable renewable energy. *Energy* 2019;180:258–71.
- [16] Maio FD, Colli D, Zio E, Liu T, Tong J. A multi-state physics modeling approach for the reliability assessment of nuclear power plants piping systems. *Ann Nucl Energy* 2015;80:151–65.
- [17] Qian G, Chou H-W, Niffenegger M, Huang C-C. Probabilistic aging and risk analysis tools for nuclear piping. *Nucl Eng Des* 2016;300:541–51.
- [18] Szega M. An improvement of measurements reliability in thermal processes by application of the advanced data reconciliation method with the use of fuzzy uncertainties of measurements. *Energy* 2017;141:2490–8.
- [19] Downey A, Lui Y-H, Hu C, Laflamme S, Hu S. Physics-based prognostics of lithium-ion battery using non-linear least squares with dynamic bounds. *Reliab Eng Syst Saf* 2019;182:1–12.
- [20] Santhosh TV, Gopika V, Ghosh AK, Fernandes BG. An approach for reliability prediction of instrumentation & control cables by artificial neural networks and Weibull theory for probabilistic safety assessment of NPPs. *Reliab Eng Syst Saf* 2018;170:31–44.
- [21] Almoudi L, Wang B. A review of the state-of-the-art in wind-energy reliability analysis. *Renew Sustain Energy Rev* 2018;81:1643–51.
- [22] Su H, Zhang J, Zio E, Yang N, Li X, Zhang Z. An integrated systemic method for supply reliability assessment of natural gas pipeline networks. *Appl Energy* 2018; 209:489–501.
- [23] Chiacchio F, D'Urso D, Famoso F, Brusca S, Aizpurua JI, Catterson VM. On the use of dynamic reliability for an accurate modeling of renewable power plants. *Energy* 2018;151:605–21.
- [24] Babykina G, Brinzei N, Aubry J-F, Deleuze G. Modeling and simulation of a controlled steam generator in the context of dynamic reliability using a stochastic hybrid automaton. *Reliab Eng Syst Saf* 2016;152:115–36.
- [25] Chiacchio F, D'Urso D, Manno G, Compagno L. Stochastic hybrid automaton model of a multi-state system with aging: reliability assessment and design consequences. *Reliab Eng Syst Saf* 2016;149:1–13.
- [26] Liu J, Zio E. System dynamic reliability assessment and failure prognostics. *Reliab Eng Syst Saf* 2017;160:21–36.

- [27] Solanki RB, Kulkarni HD, Singh S, Verma AK, Varde PV. Optimization of regression model using principle component regression method in passive system reliability assessment. *Prog Nucl Energy* 2018;103:126–34.
- [28] Solanki RB, Kulkarni HD, Singh S, Varde PV, Verma AK. Reliability assessment of passive systems using artificial neural network based response surface methodology. *Ann Nucl Energy* 2020;144:107487.
- [29] Du Z, Chen L, Jin X. Data-driven based reliability evaluation for measurements of sensors in a vapor compression system. *Energy* 2017;122:237–48.
- [30] Martinez-Luengo M, Kolios A, Wang L. Structural health monitoring of offshore wind turbines: a review through the statistical pattern recognition paradigm. *Renew Sustain Energy Rev* 2016;64:91–105.
- [31] Pan Y, Er MJ, Li X, Yu H, Gouriveau R. Machine health condition prediction via online dynamic fuzzy neural networks. *Eng Appl Artif Intell* 2014;35:105–13.
- [32] Baptista M, Henriques EMP, de Medeiros IP, Malere JP, Nascimento Jr CL, Prendinger H. Remaining useful life estimation in aeronautics: combining data-driven and Kalman filtering. *Reliab Eng Syst Saf* 2019;184:228–39.
- [33] Tao T, Zio E, Zhao W. A novel support vector regression method for online reliability prediction under multi-state varying operating conditions. *Reliab Eng Syst Saf* 2018;177:35–49.
- [34] Yazdani M, Babagolzadeh M, Kazemitaish N, Saberi M. Reliability estimation using an integrated support vector regression – variable neighborhood search model. *J Ind Inf Integrat* 2019;15:103–10.
- [35] Li X, Ding Q, Sun J-Q. Remaining useful life estimation in prognostics using deep convolution neural networks. *Reliab Eng Syst Saf* 2018;172:1–11.
- [36] Yoo KH, Back JH, Na MG, Hur S, Kim H. Smart support system for diagnosing severe accidents in nuclear power plants. *Nucl Eng Technol* 2018;50:562–9.
- [37] Wang S-L, Fernandez C, Zou C-Y, Yu C-M, Chen L, Zhang L. A comprehensive working state monitoring method for power battery packs considering state of balance and aging correction. *Energy* 2019;171:444–55.
- [38] Sorrentino M, Accocia M, Panagrosso D, Trifirò A. Model-based energy monitoring and diagnosis of telecommunication cooling systems. *Energy* 2016;116:761–72.
- [39] Zahedi yeganeh MH, Ansarifar GR. Estimation of the poisons reactivity in the P.W. R nuclear reactor using modified higher order sliding mode observer based on the multi-point nuclear reactor model. *Ann Nucl Energy* 2018;112:158–69.
- [40] Dong Z, Liu M, Guo Z, Huang X, Zhang Y, Zhang Z. Adaptive state-observer for monitoring flexible nuclear reactors. *Energy* 2019;171:893–909.
- [41] Chen W-H, Ballance DJ, Gawthrop PJ, O'Reilly J. A nonlinear disturbance observer for robotic manipulators. *IEEE Trans Ind Electron* 2000;47:932–8.
- [42] Chen W-H, Yang J, Guo L, Li S. Disturbance-observer-based control and related methods—an overview. *IEEE Trans Ind Electron* 2016;63:1083–95.
- [43] Ding S, Chen W-H, Mei K, Murry-Smith DJ. Disturbance observer design for nonlinear systems represented by input-output models. *IEEE Trans Ind Electron* 2020;67:1222–32.
- [44] Han J. From PID to active disturbance rejection control. *IEEE Trans Ind Electron* 2009;56:900–6.
- [45] Freidovich LB, Khalil HK. Performance recovery of feedback-linearization-based designs. *IEEE Trans Automat Control* 2008;53:2324–34.
- [46] Su YX, Duan BY, Zheng CH, Zhang YF, Chen GD, Mi JW. Disturbance-rejection high-precision motion control of a Stewart platform. *IEEE Trans Control Syst Technol* 2004;12:364–74.
- [47] Zhao L, Yang Y, Xia Y, Liu Z. Active disturbance rejection position control for a magnetic rodless pneumatic cylinder. *IEEE Trans Ind Electron* 2015;62:5838–46.
- [48] Dong Z, Huang X, Li D, Zhang Z. Reactivity estimation based on an extended state observer of neutron kinetics. *IEEE Trans Nucl Sci* 2016;63:2691–7.
- [49] Ben-Abdenour A, Edwards RM, Lee KY. LQG/LTR robust control of nuclear reactors with improved temperature performance. *IEEE Trans Nucl Sci* 1992;39:2286–94.
- [50] Edwards RM, Lee KY, Schultz MA. State feedback assisted classical control: an incremental approach to control modernization of existing and future nuclear reactors and power plants. *Nucl Technol* 1990;92:167–85.
- [51] Wang D, Ma C, Dong D, Lin J. Chinese nuclear heating test reactor and demonstration plant. *Nucl Eng Des* 1992;136:1–8.
- [52] Wang D, Zhang D, Dong D, Gao Z, Li H, Lin J, Su Q. Experiment study and operation experience of the 5MW nuclear heating reactor. *Nucl Eng Des* 1993;143:9–18.
- [53] Dong Z, Pan Y. A lumped-parameter dynamical model of a nuclear heating reactor cogeneration plant. *Energy* 2018;145:638–56.
- [54] Dong Z. PD power-level control design for PWRs: a physically-based approach. *IEEE Trans Nucl Sci* 2013;60:3889–98.
- [55] Dong Z, Huang X, Feng J. Water-level control for the U-tube steam generator of nuclear power plants based on output feedback dissipation. *IEEE Trans Nucl Sci* 2009;56:1600–12.